Annu. Rev. Biochem. 2005. 74:833–65
doi: 10.1146/annurev.biochem.73.011303.074112

STRUCTURAL STUDIES BY ELECTRON TOMOGRAPHY: From Cells to Molecules

Vladan Lučić, Friedrich Förster, and Wolfgang Baumeister
Department of Structural Biology, Max Planck Institute of Biochemistry, D-82152 Martinsried, Germany; email: vladan@biochem.mpg.de, foerster@biochem.mpg.de, baumeist@biochem.mpg.de

Key Words cryo, electron microscopy, image analysis

■ **Abstract** Electron tomography (ET) is uniquely suited to obtain three-dimensional reconstructions of pleomorphic structures, such as cells, organelles or supramolecular assemblies. Although the principles of ET have been known for decades, its use has gathered momentum only in recent years, thanks to technological advances and its combination with improved specimen preparation techniques. The rapid freezing/freeze-substitution preparation is applicable to whole cells and tissues, and it is the method of choice for ET investigations of cellular ultrastructure. The frozen-hydrated preparation provides the best possible structural preservation and allows the imaging of molecules, complexes, and supramolecular assemblies in their native state and their natural environment. Devoid of staining and chemical fixation artifacts, cryo-ET provides a faithful representation of both the surface and internal structure of molecules. In combination with advanced computational methods, such as molecular identification based on pattern recognition techniques, cryo-ET is currently the most promising approach to comprehensively map macromolecular architecture inside cellular tomograms.

CONTENTS

1. INTRODUCTION

Tomography aims to produce three-dimensional images (tomograms) of objects. The first approaches to image biological objects three-dimensionally were tomograms (from Greek $\tau\varepsilon\mu\nu\acute{\varepsilon}\iota\nu$, to section) in the original meaning of the term. That is, objects were cut in slices and imaged. Methods that are now referred to as tomographic do not require physical sectioning anymore because they rely on an entirely different principle.

Structural investigations of biological material at all levels from molecules to cells provided innumerable contributions to the understanding of their function. Cells possess rich structural organization between the molecular and cellular levels. Molecular complexes are functional units that perform specific tasks. Some, such as ribosomes, are robust enough to withstand biochemical isolation and purification procedures, and these complexes can be studied by established structural biology methods. Others, such as G protein–associated complexes, assemble only transiently and/or are held together by weak forces. They tend to be structurally and functionally more variable and undergo significant rearrangement in response to various signals. Ideally, their structure should be studied in their native environment. In addition, these functional units may be organized into dynamic supramolecular assemblies with an even more diverse architecture. Electron tomography (ET) can provide a bridge between structural studies at the molecular and cellular levels. It allows the investigation of the molecular architecture of complexes and assemblies in their natural, cellular environment and is therefore uniquely positioned to elucidate their structure-function relationship.

ET is based on a principle first discovered by Radon (1): A tomogram (three-dimensional reconstruction) can be retrieved from the projections of an object. This principle was further developed and put into practice in 1968 (2, 3; reviewed in 4) to become the basis for all forms of three-dimensional electron microscopy (EM): electron crystallography, single-particle analysis, and ET.

The combination of ET with improvements of specimen preparation techniques allowed researchers to overcome some of the notorious artifacts of EM preparation methods, leading to the recent increased resurgence of ET. Investigation of cellular components in their native state by EM requires the specimen to be investigated in the hydrated state. In an early attempt to prevent water evaporation from a hydrated specimen in the vacuum of the electron microscope, a differentially pumped hydration chamber was designed in which the specimen could remain in a saturated water vapor atmosphere while staying inside the microscope (5). Lowering the specimen temperature to a point at which water evaporation becomes negligible is another approach to solve the same problem (6). Showing that the structure of a frozen catalase crystal is preserved to atomic resolution (7) was an important breakthrough. However, only the vitrification of a thin specimen by plunging it into liquid ethane (cryopreparation), thereby avoiding formation of ice crystals and thus the damage they cause, allowed the investigation of a specimen in the fully hydrated, close to physiological form (reviewed in Reference 8).

The first tomograms were recorded manually. However, cryopreparation suffered from radiation damage unavoidably caused by the high electron dose used during manual recording. The sensitivity of the biological specimen in ice to electron damage requires the images to be recorded under low electron dose conditions. The advent of automated data acquisition procedures (9–11) allowed recording under low-dose conditions and therefore made the ET of cryo-prepared specimens possible.

2. TECHNICAL ASPECTS

2.1. Principles of Electron Tomography

The development of ET required contributions from various different fields. On the theoretical side, ET needed a quantitative understanding of the imaging process in the electron microscope and the development of suitable three-dimensional reconstruction algorithms. The technical advances comprise the engineering of suitable imaging equipment as well as automated data acquisition programs. Possibly the major challenge for the future remains the quantitative evaluation of tomograms.

2.1.1. IMAGE FORMATION IN TRANSMISSION ELECTRON MICROSCOPY Owing to the large depth of focus of a transmission electron microscope (TEM), an electron micrograph is essentially a two-dimensional projection of objects under scrutiny. The image formation differs for different specimen preparations. The contrast of stained specimens mainly arises from amplitude contrast (12, 13), and so the projections of the electrostatic potential of the specimen are proportional to the logarithm of micrograph pixel values.

Phase contrast is a dominant contrast-forming mechanism for nonstained specimens, such as frozen hydrated specimens (14). Here, the relation of specimen and electron micrograph is more complex: The micrograph is a projection of the specimen's electrostatic potential, convoluted with the inverse Fourier transform of contrast-transfer function (CTF), in which CTF describes the imaging conditions and the TEM properties. The microscopist can influence the CTF mainly by choosing a defocus value. Small defocus values ensure that the information about fine details is retained, but this is at the expense of obtaining low contrast images. The exact value of defocus used places a limit on the obtainable resolution (at a resolution that is somewhat lower than the first zero of CTF). To be precise, bands of higher frequency information are present in micrographs, but they are hard to interpret because the bands have alternating contrast. The restoration of the true projection is rarely done in ET as it requires an exact determination of CTF, a difficult task for low signal-to-noise ratio (S/N) micrographs of nonstained preparations.

2.1.2. INSTRUMENTATION A typical ET setup consists of a TEM equipped with a field-emission gun (FEG) and a computer-controlled stage, a charge-coupled device (CCD) camera, and possibly an energy filter. FEG microscopes produce an

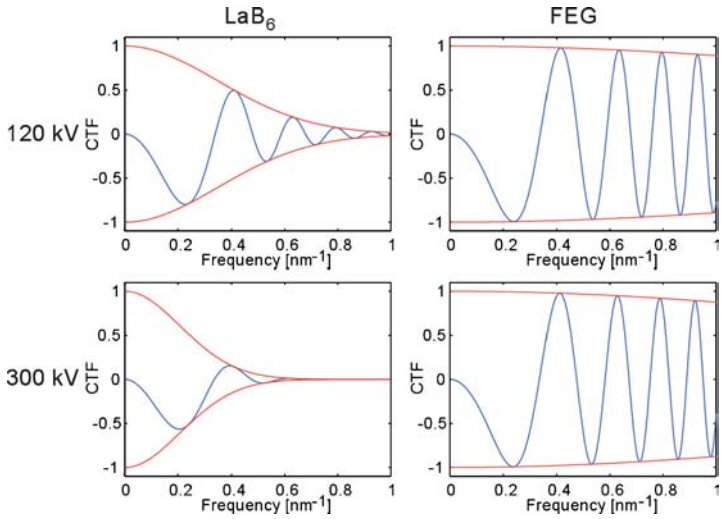

Figure 1 Theoretical CTFs (*purple*) and their envelopes (*red*) for LaB_6 TEMs (*left column*) and FEG instruments (*right column*) for acceleration voltages of 120 kV (*top row*) and 300 kV (*bottom row*). The increased spatial coherence (illumination aperture $\alpha = 0.2$ mrad and $\alpha = 0.02$ mrad for LaB_6 and FEG, respectively) and improved temporal coherence (energy width of the incident beam $\Delta E = 3$ eV and $\Delta E = 0.8$ eV for LaB_6 and FEG, respectively) of FEG instruments lead to smaller attenuation of the CTF. Defocus values (-2.6 μm at 120 kV and -4.5 μm at 300 kV) were chosen such that the first zero of the CTF occurs at $(3\ \text{nm})^{-1}$.

electron beam of high spatial and temporal coherence. The minimal attenuation of the CTF envelope, as a function of spatial frequency, is obtained with FEG-equipped microscopes and leads to preservation of high-resolution information. Imaging at intermediate (200–600 kV) and high voltages ($\geq$800 V) has two advantages: Electrons can penetrate thicker samples, which makes imaging of cells or organelles possible. Moreover, the attenuation of the CTF envelope is smaller, improving the achievable resolution (Figure 1). Therefore, imaging at voltages below 200 kV is suitable for thin specimens, whereas thicker specimens inevitably require intermediate or high voltages.

Energy filtering is a viable way to circumvent the effects of the chromatic aberration of TEMs, thus increasing the contrast. The interaction of electrons with thick ($>$200 nm) specimens inevitably produces many inelastic scattering events, leading to a wide energy distribution of the scattered electrons and strong blurring. Energy filters operating in "zero-loss" mode eliminate electrons and thus allow imaging of thick specimens at significantly higher S/N (15). They are indispensable for tomography of whole ice-embedded cells or other objects of 0.5–1 μm thickness (16, 17).

In ET, images are recorded on a CCD camera, as opposed to film, owing to the necessity of using automated data acquisition, which in turn requires the immediate

availability of images. CCD cameras offer other advantages: easy handling, high linearity of the signal as a function of the number of incoming electrons, and a large dynamic range.

Electrons are first converted to photons in a scintillator. The photons are then transmitted to the CCD chip via fiber coupling. Backscattering of electrons into the scintillator degrades the performance of CCD cameras. Furthermore, because of the small scattering cross section of the scintillator for high-energy electrons, relatively thick scintillators have to be used to achieve a sufficient yield of photons, leading to a spread of the signal generated by an incoming electron (18). As a result, the performance of CCD cameras decays rapidly for higher spatial frequencies and for higher accelerating voltages. Whereas the performance of CCD cameras is satisfactory for voltages below 200 kV, it is currently a major limiting factor for resolution at intermediate and high voltages.

Alternatively, photons are transferred to the CCD chip via a lens system in a lens-coupled camera, allowing the photons arising from one electron to be focused, which improves the performance of the camera (19). Although the gain in resolution is at the expense of collection efficiency, the use of lens-coupled systems promises to significantly improve digital imaging with high-energy electrons (18). Nevertheless, the optimum recording device for EM detects electrons directly, providing the long-term solution for digital TEM imaging (20).

2.1.3. DATA ACQUISITION The aim of data acquisition is the recording of a tilt series, i.e., a series of micrographs (projections) of the specimen recorded at different tilt angles (Figure 2). There are two fundamental requirements the tilt series has to fulfill: The object of interest has to be kept within the field of view, and all projections have to be acquired under comparable imaging conditions.

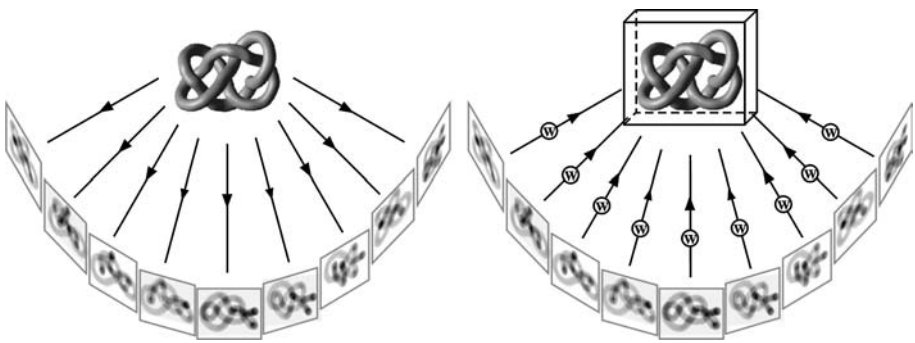

Figure 2 Principle of tomography. (*left*) Projections of the specimen were recorded from different directions by tilting the specimen holder. (*right*) The three-dimensional reconstruction of the sample is obtained most commonly by backprojection into a common three-dimensional reconstruction body.

Mechanical inaccuracies of the specimen holder cause specimen movement during tilting, which requires appropriate compensating adjustment. Because manual adjustment generally requires extensive exposure of the sample to the electron beam, the automation of the acquisition process was crucial to acquire a tilt series under low-dose conditions.

The development of the first procedures for automated data collection has changed the perspective of ET in a profound manner (9, 10, 21). In fact, automation was indispensable for the acquisition of the first cryotomograms (16, 22). The automated acquisition of a tilt series requires three basic steps (10, 11): tracking, autofocusing, and exposure (recording a projection). In the tracking procedure, a micrograph of a very low dose is recorded prior to the final exposure to determine the lateral displacement of the specimen compared to the previous tilt angle. The autofocusing step compensates for the change of defocus because of specimen movement in the beam direction. The autofocusing procedure determines the defocus by comparing micrographs acquired at different beam tilts (23, 24). These two steps are carried out under low-dose conditions at positions that are shifted along the tilt axis in reference to the exposure location to minimize the electron dose received by the object of interest.

The recording of a tilt series following this procedure is time consuming because it often comprises more than 100 projections. Efforts to reduce the recording time by predicting the specimen movement typically succeeded only at room temperature (25). However, the development of highly stable, eucentric specimen holders led to the development of a faster tilt series acquisition procedure applicable to cryo conditions (26).

2.1.4. RECONSTRUCTION ALGORITHMS The three-dimensional reconstruction of an object from its projections involves two steps: First, the different micrographs have to be aligned to a common coordinate system, and second, the aligned micrographs have to be merged into a tomogram.

Alignment of the different projections compensates for small specimen movements within the image field. An alignment procedure has to determine the angle of the tilt axis and the lateral shifts due to the limited precision of the tracking procedure and, possibly, other changes, such as magnification changes or image rotation. Projections can be aligned by cross correlation (27) or by the common lines method (28). However, those methods are typically noise sensitive and only work well for a limited class of specimens, such as high-contrast or paracrystalline objects (29). Another alignment method based on adding fiducial markers (typically colloidal gold) to the specimen is more common. The coordinates of these markers on each projection are determined manually or automatically. An alignment model is calculated using least-squares procedures [e.g., (30)] that minimize the alignment error as a function of the lateral translations and the angle of the tilt axis. Additional parameters, such as magnification change, image rotation, and tilt angle, can also be incorporated into the model. However, some of these additional parameters may have large uncertainty, and so several gold

markers may be needed to determine all of them with high accuracy. Alternatively, a cross-correlation alignment method based on the iterative optimization of the consistency of a reconstruction and its projections could be developed. Such an approach would be more elaborate and computationally demanding, but it could be parallelized painlessly.

The reconstruction of the tomogram is performed after the alignment of the projections. The possibility of recovering three-dimensional data from projections can be explained in Fourier space: The Fourier transformation of a projection corresponds to a slice in the three-dimensional Fourier space of the object imaged. The first three-dimensional reconstructions of EM data (2) used a Fourier space approach, amounting to interpolation in the Fourier space. Because this is a notoriously difficult problem, the real space-based reconstruction methods are commonly used (reviewed in Reference 31).

The most common reconstruction method in ET is the weighted backprojection (reviewed in Reference 32). Backprojection is a conceptually simple approach in which the projections are projected back to form a three-dimensional reconstruction (Figure 2). However, because of uneven sampling in the Fourier space (Figure 3), the low frequencies are artificially enhanced, requiring weighting of projections prior to backprojection to obtain a faithful reconstruction. Two different schemes can be distinguished: analytical and exact. In both cases, weighting is done in the Fourier space. The analytical weighting function is proportional to the frequency in the direction perpendicular to the tilt axis, and it becomes equivalent to the exact weighting for an infinitely small tilt increment. Exact weighting procedures estimate the sampling density in Fourier space using the characteristic size of the object of interest in the specimen (33).

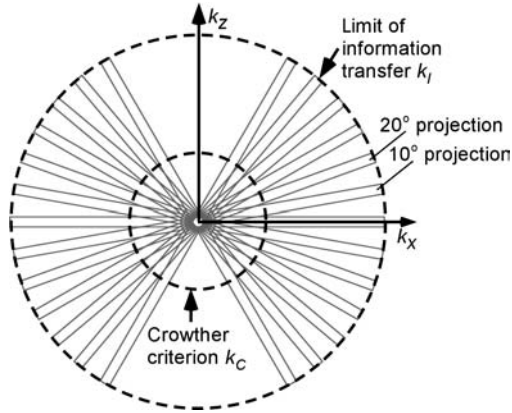

Figure 3 Data sampling in Fourier space. A projection of an object with thickness d corresponds to a central slice of thickness $1/d$ in Fourier space. Therefore, the three-dimensional information of the specimen (outside of the missing wedge) is gathered homogeneously up to frequency k_C (Crowther criterion).

Alternatively, algebraic reconstruction techniques (ART) can be used (34). Despite initial criticism (35), ART has been established as a viable method for three-dimensional reconstruction. ART formulates the projections of an unknown potential in a set of algebraic equations and aims to invert this equation system. An approximate inversion is achieved by different iterative algorithms. In principle, ART and various closely related iterative techniques offer two major advantages: (*a*) proper weighting is determined consistently, i.e., ART is parameter free in that sense, and (*b*) constraints can be incorporated easily, which can be enticing (reviewed in Reference 36). Powerful constraints can lead to significant improvements of the resulting reconstructions, but these are typically not available for pleomorphic specimens. On the contrary, the introduction of strong but erroneous constraints imposes severe artifacts. A strong constraint constitutes information on the outer shape of the three-dimensional object, which is an implicit constraint of ART (37). However, complex biological specimens, such as cells, normally do not allow researchers to take advantage of this powerful constraint in ET. Other established constraints, such as limited basis functions (e.g., "blobs") (38) or variance minimization (37) can lead to the reduction of artifacts compared to the weighted backprojection, but these improvements are merely incremental. Drastic improvements, as claimed by the introduction of "maximum entropy" constraints (39), are equivocal and remain to be proven.

Nevertheless, ART and other iterative reconstruction algorithms may offer advantages over the weighted backprojection. The development of computationally fast implementations as reported in (40) might encourage the future use of ART in ET.

2.1.5. ANGULAR SAMPLING AND TILTING STRATEGIES The idea behind the tomographic approach, i.e., that more information can be obtained from a tomogram than from a single projection by using the same electron dose, is precisely stated by the dose-fractionation theorem; in both cases, each volume element is in principle described with the same statistical significance (41, 42). Merging the information of many volume elements in a plane element of a single micrograph using the entire dose, ET makes it possible to distinguish the information contributed by different volume elements. However, the value of this additional data depends on the resolution achieved; the additional information in the third dimension is only useful when higher resolution allows different volume elements to be distinguished (43).

One of the factors limiting the resolution in a tomogram is the number of projections (N) comprising a tilt series. The Crowther criterion (44) provides an estimate for the obtainable resolution (r) of an object having size (d) in the direction of the electron beam:

$$r = \frac{\pi d}{N}.$$

This equation is based on the fact that the Fourier transformation of a projection corresponds to a central slice of the Fourier transformation of the three-dimensional

reconstruction (Figure 3). The thickness of the slice is reciprocally proportional to d. According to this equation, high resolution can be obtained for macromolecules and other small objects. However, for most applications, the molecular resolution is not limited by the Crowther criterion but by the structural preservation of specimen or the noise (see below). The limited significance of the Crowther criterion as a resolution measure for cellular tomography also becomes apparent because the size of the recorded object is poorly defined; in fact, a cell consists of objects of various sizes. Nevertheless, the Crowther criterion remains an important means of interpreting tomograms.

The Crowther relation was derived for specimens that are circular and perpendicular to the tilt axis and for a constant tilt increment. For slab geometry of the specimen, Saxton et al. (45) proposed a variation of the tilt increment to ensure even sampling. This scheme is rarely used because a large part of the overall electron dose is spent on projections at high tilt angles that have low S/N, and this disadvantage can outweigh its benefits (46).

In ET, the tilt range is limited to $\pm 70^\circ$ by the design of the specimen holders, leaving a "missing-wedge," an unsampled wedge-shaped region in Fourier space (Figure 4), and causing nonisotropic resolution. As a consequence, reconstructed objects appear elongated in the beam direction, and some structural elements are not resolved at all. Surfaces, such as membranes, are resolved over a wide range of orientations, whereas they are hardly resolved if they are perpendicular to the plane defined by the beam direction and the tilt axis (see Figure 4, *left*). The acquisition of a double-tilt series can correct this shortcoming; two single-tilt series of the objects are recorded during which the specimen is rotated by 90° around the beam direction after the first series. This acquisition procedure samples the structural factors of the objects more isotropically, so only a pyramid-shaped region in Fourier space

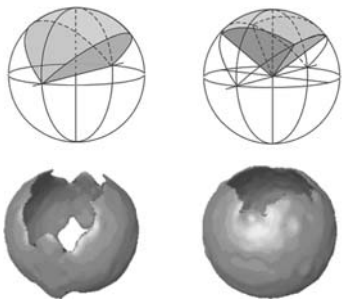

Tilt range	Single	Double
±70°	78%	93%
±60°	67%	84%
±45°	50%	67%

Figure 4 Single- and double-axis tilting. The upper illustrations show schematically the sectors in the Fourier domain that remain unsampled because of the limited tilt range. In single-axis tilting (*left*), there is a "missing wedge," in double-axis tilting (*right*), a "missing pyramid." The table contains percentages of the Fourier space that are covered for different tilting schemes. The missing information in real space is illustrated below.

remains unsampled (see Figure 4, *right*). Consequently, although the maximum resolution is not increased, the achievable resolution is more isotropic. For medium resolution studies in particular, the improved isotropy of the resolution outweighs the slightly lower S/N obtained by the double-tilt method.

The acquisition of a double-tilt series requires physical rotation of the grid in the holder. It can be performed outside the TEM for noncryo samples, but cryo samples require a grid-rotating device within the TEM to avoid contamination. The development of such a specimen holder led to the acquisition of the first double-tilt cryotomograms (47).

In the first alignment of the double-tilt series, the two data sets were merged by determining the rotation and translation vector of the coordinate systems established for both series independently (48). The final reconstruction was performed using exact weighting of the micrographs in Fourier space. Another approach, based on the general linear transformation, was used to align the reconstructions of the two single-tilt series to make the final reconstruction (46). This alignment provides better compensation for the imperfections of the tilt geometry and for radiation-induced specimen shrinkage.

2.1.6. IMAGE ANALYSIS AND INTERPRETATION The interpretation of tomograms at the ultrastructural level requires decomposition of a tomogram into its structural components, e.g., the segmentation of intracellular membranes or the assignment of organelles. Currently, a manual assignment of features is commonly used because human anticipation is still superior in most cases to available segmentation algorithms (see Figure 5*b*), although machine-based segmentation is in principle more objective (49, 50).

Cryopreparation provides the ability to interpret tomograms at the molecular level. However, the analysis and three-dimensional visualization are hampered by low S/N. In order to increase the S/N, so-called denoising algorithms have been developed (reviewed in Reference 51). These algorithms aim to identify noise and remove it from the tomogram, but in practice, they also remove a certain fraction of the signal, resulting in data with reduced information but higher S/N. The simplest denoising techniques used diverse linear filtering operations, such as a simple low-pass filtering in Fourier space. Better signal preservation can be achieved by nonlinear filtering algorithms, such as nonlinear anisotropic diffusion (NAD) (52, 53) or bilateral filtering (54). NAD is particularly useful for the visualization of the ultrastructural features because it can enhance features such as membranes. In addition, these filters may provide better signal preservation, which is suitable for visualization at the molecular resolution level. Denoising based on the wavelet transformations (55) preserves high-resolution information relatively well, but its immense computational effort currently favors the former approaches.

Cryo-ET enables us to resolve large macromolecular complexes such as the 26S proteasome inside intact cells (56). High-resolution structures of numerous macromolecules are available from X-ray crystallography or NMR. The purpose of

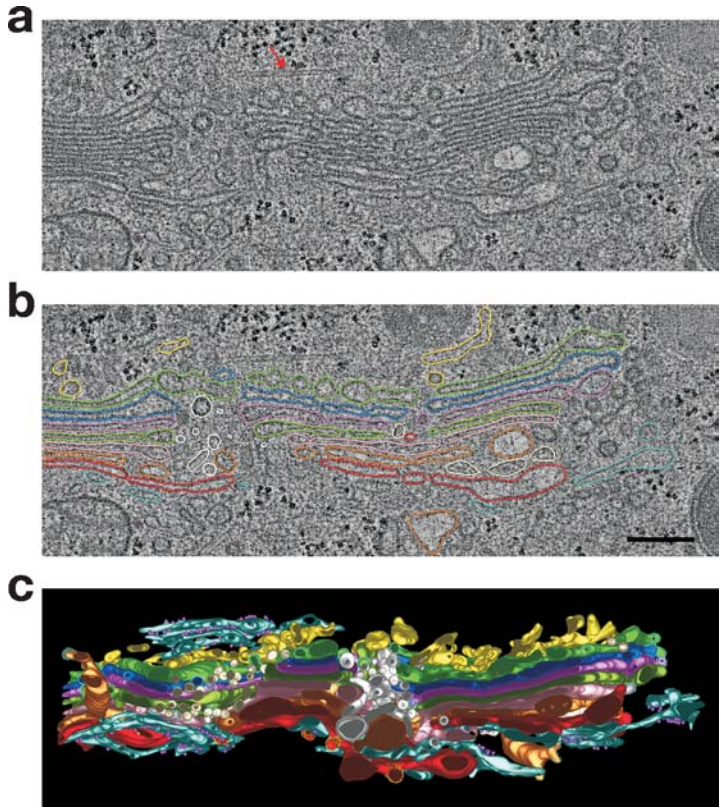

Figure 5 Reconstruction of a portion of the Golgi ribbon, (from Reference 81, with permission). (*a*) Membranes of individual Golgi and ER cisternae are clearly shown. (*b*) Manual segmentation of cisternae. (*c*) Surface-rendered membrane compartments. Scale bar 250 nm.

many ongoing structural genomics projects is to generate a comprehensive library of protein structures. Therefore, molecular recognition is the task of locating a priori known structures in the context of cells or other complex biological samples rather than clarifying structurally novel features, which is the purpose of denoising. Mapping of macromolecules on the basis of their structural signature requires the quantitative comparison of tomogram data to a library of macromolecular structures (Figure 6). Ideally, the search of tomograms should be exhaustive and would reveal a cellular atlas of resolvable macromolecules. Simulations and experiments with "phantom cells," i.e., liposomes encapsulating macromolecules, indicated that such an approach is feasible (57, 58). The information concerning the spatial relationship of different complexes complements the data of other proteomic methods and will be indispensable for structural proteomic approaches (59).

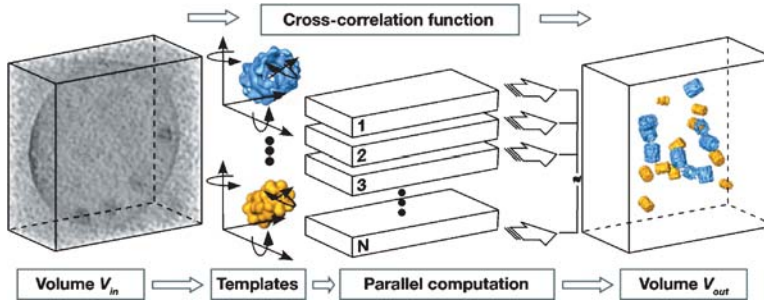

Figure 6 Identification of individual macromolecules based on their structural signature. The template-matching approach uses known structures (e.g., obtained from X-ray crystallography or NMR) to search the entire volume of the tomogram systematically for matching patterns by a cross-correlation approach. The search procedure is parallelized to make it computationally feasible.

The most common molecular detection algorithm is a locally normalized, matched filter, introduced in a different context (60, 61). It was modified to account for the missing-wedge effect (58) and applied to cryotomograms (58, 62). These applications demonstrated that it is feasible to identify large macromolecular complexes (>500 kDa) within cryotomograms with high fidelity. Furthermore, the high computational demand of template matching is significantly reduced by the parallelization.

The information an individually resolved macromolecule contains is limited because of the low electron dose and the missing-wedge effect. Averaging techniques aim to overcome the dose limitation of resolution by explicit averaging of different reconstructions from the same particle. Iterative algorithms are used to align subtomograms of arbitrarily oriented copies of a particle and obtain a consistent average (63). Medium resolution (2–3 nm) structures of the Thermosome and Tricorn could be obtained from cryotomograms of purified complexes (63, 64). Generally, the resolution from cryo-ET is inferior to conventional single-particle reconstructions, which use two-dimensional projections of particles recorded on film to obtain three-dimensional structures. Considering the aforementioned dose fractionation theorem (41), the higher information content of tomograms should favor averaging of tomograms over averaging from projections. However, the low resolution of CCD cameras in respect to film, the alignment error of the micrographs prior to three-dimensional reconstruction, and the current inability to reliably correct for the CTF argue against averaging of tomograms. Nevertheless, cryo-ET can provide medium-resolution structures of protein complexes without using extensive purification procedures (65). Furthermore, structures obtained by cryo-ET can be used as starting models that are refined by single-particle techniques (63) or can be combined with other higher resolution structural techniques to provide comprehensive descriptions of molecular complexes.

2.2. Specimen Preparation in ET and Related Techniques

EM has a long history in the development of specimen preparation techniques. Some of the older techniques are notorious for their artifacts. The strengths and weaknesses of various techniques not only determine their applicability to different specimen types (such as isolated molecular complexes or whole cells) and the type of structural information that can be retrieved, but also determine the limitations to be considered when interpreting the data. In addition, we describe a few techniques that are yet to show their full benefit for ET.

2.2.1. STAINING Staining with heavy metal salts is a commonly used method for increasing the contrast in EM. In positive staining, the stain forms a complex with the organic material, giving it a dark (stained) appearance. In negative staining, the heavy metals accumulate around the molecules of the specimen and also penetrate the cavities, where they replace water. The specimen is represented by the stain-excluding area; it appears light, surrounded by the dark envelope of heavy metals. However, an intricate combination of positive and negative stains is often obtained, which is difficult to disentangle. If used without fixation, it is not suitable for larger specimens. Also, although staining greatly improves the contrast, what is seen on the electron micrographs is the stain and not the biological material.

2.2.2. CONVENTIONAL PREPARATION INVOLVING CHEMICAL FIXATION AND PLASTIC EMBEDDING In the conventional preparation, the specimen is first chemically fixed; then dehydrated in organic solvents, embedded in a suitable resin or plastic; and sectioned into slices. The slices are stained to increase contrast. This preparation is often used for EM studies of sectioned cells and tissues.

For ET, the slices are usually 200–500 nm thick. This differs from the thin (20–100 nm) sections usually used in the serial section reconstruction, in which single images of individual thin sections are computationally merged to obtain a three-dimensional reconstruction, limiting the resolution in the z direction to the slice thickness.

Chemical fixation and dehydration are harsh treatments that promote leakage of some cytoplasmic components and cause aggregation artifacts. Furthermore, structural rearrangements within the specimen may occur during the slow course of chemical fixation. Considerable effort was spent on optimizing this preparation; however, before the advent of cryopreparation, there was no reliable reference to allow verification of structural preservation.

2.2.3. RAPID FREEZING (CRYOFIXATION) Preservation of specimen by rapid freezing is currently the best method for structural preservation. The specimen is frozen rapidly enough to reach the temperature (below -140°C) at which the ice is in a vitreous state before it can form crystals. The vitreous ice is amorphous, similar to a liquid but with high viscosity. Formation and growth of ice crystals, which normally occurs at temperatures below 0°C, under a slow freezing processes can

damage the specimen. It also leads to dehydration, which causes increased solute concentrations, eventually leading to structural changes of proteins. Rapid freezing essentially immobilizes all constituents of a specimen before a significant rearrangement occurs and, therefore, preserves the specimen in a near physiological state.

Specimens up to 10 μm can be frozen by plunge freezing: The specimen, immersed in a thin film of water on an EM grid, is plunged into liquid ethane or propane. High-pressure freezing (HPF) is suitable for thicker specimens (up to a few hundred μm). The specimen is pressurized and at the same time cooled by jets of liquid nitrogen, thus hindering the formation of ice crystals (66).

2.2.4. RAPID FREEZING/FREEZE-SUBSTITUTION (RF/FS) AND PLASTIC EMBEDDING PREPARATION The popularity of this method is due to recent improvements in design, availability of high-pressure freezers, and its usefulness in the investigation of thick specimens, such as cells and tissues. The specimen is rapidly frozen (usually by HPF) and then undergos the freeze-substitution procedure, whereby water is substituted by an organic solvent containing chemical fixatives at temperatures around -80°C. The sample is then embedded in resin or plastic, preferably at a low temperature (-40°C) by a low-temperature resin or at room temperature by a conventional one. Sectioning and poststaining are done as in the conventional preparation.

The main improvement over the conventional sample preparation is that the dehydration procedure at room temperature is avoided, and thus, structures are better preserved. Also, because the initial cryofixation step is rapid, this preparation allows the investigation of processes occurring at a timescale of tens of seconds to minutes. A quantitative assessment of artifacts caused by chemical fixation and dehydration at room temperature in a study comparing RF/FS with the conventional preparation showed significant distortions and rearrangements of internal membranes, especially tubular protrusions, during the conventional preparation (67) (Figure 7).

Although certainly a step ahead of the conventional preparation, RF/FS still causes aggregation artifacts (68). The resolution has been empirically estimated to 6 nm, probably limited by stain rearrangement, formation of stain aggregates during electron irradiation (thick sections require a high electron dose), as well as the inaccuracy with which stain represents the specimen (69). Therefore, specimen preparation by RF/FS allows investigation of whole cells and tissues and provides good contrast and faithful representation of the membranous structures and larger supramolecular structures, but it does not reach the resolution needed for a reliable interpretation at the molecular level.

2.2.5. CRYOPREPARATION AND CRYOSECTIONING In cryopreparation, the specimen is simply rapidly frozen by plunge freezing, without compromising it by further preparation. It is investigated in the frozen-hydrated state, i.e., surrounded by water molecules in an organization similar to liquid water (8). Cryo-ET is geared toward

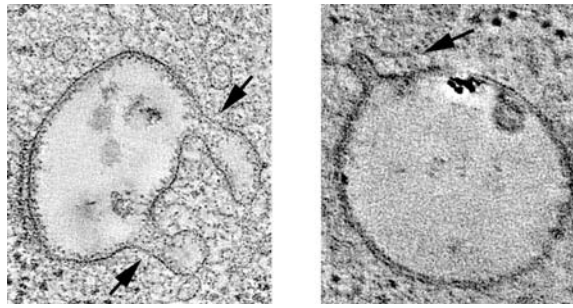

Figure 7 Influence of chemical fixation on the morphology of early endosomes (from Reference 67 with permission). Tubular protrusions (*arrows*) are enlarged in tomographic slices of the conventionally prepared early endosomes (*left*), in comparison to the the RF/FS prepared material (*right*).

the structural characterization of macromolecular complexes, which are either isolated or in a cellular environment. Suitable specimens are relatively thin, up to 500 nm, including isolated molecular complexes, small cells, and thin parts of larger cells. The specimen is kept on the EM grid for a few seconds before it is frozen, and so the surface tension of water may induce flattening in the direction perpendicular to the grid. The term "cryopreparation" is sometimes used for specimen preparations that involve freezing but also includes other preparation techniques. "Preparation of frozen-hydrated specimen" may be an alternative to the simpler cryopreparation that we chose to use.

Sections of rapidly frozen specimen in the frozen-hydrated state are obtained at low temperatures by cryosectioning. This method potentially combines the advantages of the above preparation techniques: It is applicable to whole cells and tissues, and it provides the best available preservation. Thus ET of cryosections is suitable for the investigation of molecular structure in the cellular environment. However, cryosectioning is still a challenging task despite recent progress (70). Known artifacts, such as knife marks, crevasses, and compression, further complicate three-dimensional reconstruction and interpretation. Even though we say that cryosectioning is currently an art form practiced in only few labs, we expect it to gain importance in the future.

In both preparations, the biological material is observed directly, without staining artifacts, and the membranes appear smooth. Cytoplasmic particles such as ribosomes were shown to be dispersed uniformly in the cryo sections, but these particles formed aggregates and compact clusters in the conventional preparation and showed an intermediate state in the RF/FS preparation (68). The difference is even more striking at the molecular level: Cryo sections of epidermal desmosome show straight and regularly ordered cadherin molecules, completely unlike their bent and irregular appearance in RF/FS (Figure 8) (71, 72).

Unlike the surface-only information obtained with stained specimens, cryotomograms contain information about both the surface and the internal structure of

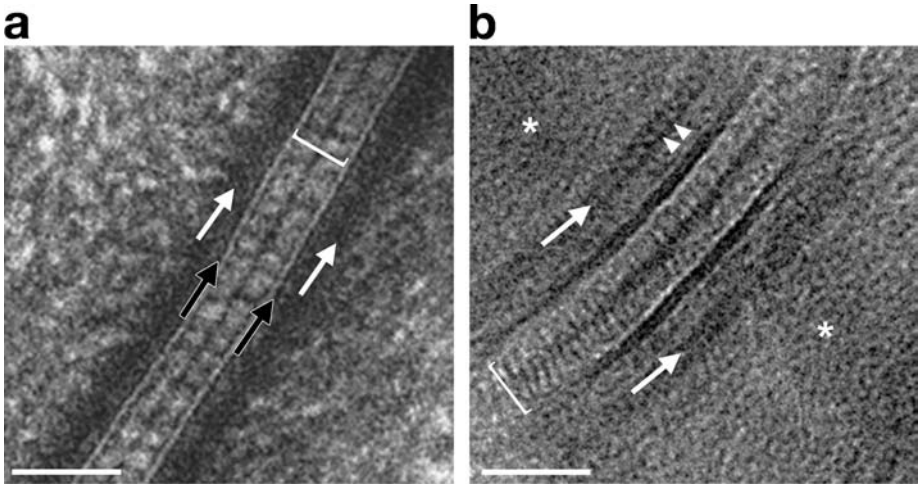

Figure 8 Comparison of the RF/FS and cryopreparations (from Reference 71, with permission). (*a*) Epidermal desmosome prepared by the RF/FS procedure. Extracellular structures appear disordered, and there is no information about intracellular structures. (*b*) Cryosection of epidermal desmosome. Extracellular structures are highly ordered, and there is a wealth of intracellular structural information. Square bracket, extracellular space; white arrows, intracellular plaques. Scale bar 50 nm.

the molecules, the latter being very useful for advanced computer-processing techniques. Docking of high-resolution structures and molecular identification based on structural signature should be performed using artifact-free three-dimensional maps and not on speckles with high contrast but unknown origin.

Because of its superb structural preservation and the ability to produce three-dimensional maps of molecules and complexes, cryopreparation is arguably the preparation of choice for ET investigation at the molecular level, and so the amount of information that is present in a cryotomogram is enormous.

2.2.6. LABELING Immunolabeling in EM is traditionally done on thin sections prepared by the Tokuyasu method (73). It provides good antigenicity, unlike the RF/FS method, but suboptimal structural preservation (74, 75). To adapt immunolabeling for ET of thick sections, preparation methods incorporating improvements that allow reliable labeling and provide good structural preservation are needed.

In cryo-ET of whole cells, immunolabeling of extracellular epitopes is possible using standard techniques. However, intracellular labeling requires innovative approaches based on noninvasive genetic manipulations. Ideally, these approaches would allow the introduction of a label at a specific time and remove the background, as done with ReAsH compound in fluorescent microscopy (76). Still, quantification of labeling is a notoriously difficult task. It is also hard to imagine

how labeling can be made compatible with the mapping of the entire proteome of a cell. No more than two or three proteins can be identified at once, and so labeling of cells has to be repeated many times. In addition, elucidation of macromolecular architecture based on several ET labeling experiments is a challenging task because of the pleomorphic nature of macromolecular assemblies.

2.2.7. CORRELATIVE LIGHT-ELECTRON MICROSCOPY During an ET investigation, one often needs to search for a sub-μm object on a 3 mm grid. Such a search under low-dose conditions (as required in cryo-ET) can be very inefficient and time-consuming. Light microscopy (LM) can be used to bridge this gap. By locating the approximate position of the object of interest using molecules with fluorescent labels, or by identifying relatively large morphological features visible in LM and then zooming in on that region, LM could be combined with ET. This approach, nevertheless, requires further technological advances.

A great advantage of LM is that it can monitor processes in living cells. A process arrested in a suitable physiological state by rapid freezing can then be investigated by EM at a much higher resolution than in LM.

2.3. Radiation Damage, Noise, and Resolution

Radiation damage is arguably the fundamental limitation of cryo-ET. Exposure of specimens to the electron beam leads to ionization, breaking of chemical bonds, and formation of free radicals. Although these processes are not temperature dependent, the resulting damage, loss of mass, and diffusion of free radicals is. Radiation damage is greatly reduced when the specimen is investigated at liquid N temperature, below -196°C. Further cooling to liquid He temperature (4 K) is advantageous for thin samples used in electron crystallography, but it is not clear yet if this is also true for thicker ice layers used in cryo-ET (8) (reviewed in Reference 77). The electron damage at low temperatures induces a gradual loss of high resolution and ultimately bubble formation, but no mass loss.

Cryotomograms have low contrast, resulting in a low S/N. The noise originates mainly from the imperfections of the CCD cameras and from the shot noise (insufficient sampling of the electron scattering from the specimen). In principle, a cryotomogram contains information up to the resolution limits set by the instrumentation and the reconstruction procedure. Nevertheless, that information is to some extent obscured by the noise, thus limiting the usable resolution.

The dependence of the resolution on noise and electron dose was discussed in References 16, 43, 78. The dose required in an actual case may differ from the theoretical estimates given in References 12, 43 by a factor of 2 or so, because the dose depends on the accelerating voltage of the electron beam and the required level of statistical significance. Furthermore, the estimates were made for images obtained by amplitude contrast (applies to stained specimen), so they do not directly apply to images obtained by phase contrast, as is the case for cryo-ET. The detection and identification of molecules might also be improved with denoising techniques.

Considering the electron dose sensitivity of the cryo specimen and the noise dependence of resolution, ET of cryo specimens has to be done in the "low-dose" mode. In other words, the total dose the object receives during EM is kept as low as possible. In addition, most of this dose should be spent on actual recording of the images comprising a tilt series. Procedures for automated data acquisition are necessary to satisfy the latter requirement, and also to help the former, together with the microscope operator skills.

Currently, apart from the dose/noise consideration, the focus gradient at high tilt angles makes reaching resolution below 3 nm very challenging (79). Nevertheless, with the expected improvements in the design of the electron detection system (18) that will permit the calculation of the CTF and correct for it at each projection, this constraint will be lifted. Because resolution is not limited by the cryopreparation, we conclude that cryo-ET is limited by the combined effect of electron dose and noise.

At room temperature, such as in the conventional and RF/FS preparations, the most striking effect of the radiation damage is the collapse of sections owing to the loss of mass (reviewed in Reference 80). The sections shrink by 40%–50% in the direction of the beam and by 5%–10% in the plane perpendicular to it. This may not be a serious problem for two-dimensional imaging because the images are projections along the beam direction. Nevertheless, it deserves serious consideration in tomography as the progressive shrinkage of a slice during the recording of a tilt series makes it hard to perform a three-dimensional reconstruction accurately, and the shrinkage sometimes produces ambiguities in combining tomograms from neighboring sections (81). This shrinkage occurs early in the recording process, so the usual solution has been to pre-expose the specimen in order to make it shrink first and then record a tilt series (69), thus increasing the total electron dose and the dose-induced stain aggregation. Sometimes, the reconstructions are stretched in order to account for the shrinking, although it is unclear if this approach is justified, because it is not known whether the mass loss is uniform or occurs only at the surface (82). Therefore, the current resolution limits of conventional and RF/FS methods are primarily set by the inaccuracy of the representation of the native material in the tomograms (by preparation and beam-induced artifacts) and to lesser extent by instrumentation or the shot noise.

3. BIOLOGICAL APPLICATIONS

Here we review the recent applications of ET to biology. Instead of providing a comprehensive list, we concentrate on a few selected examples.

3.1. Membranous Structures

Besides allowing organelles to maintain an environment that is distinct from the cytoplasm, intracellular membranes play an important role in cellular signaling. In this section, we review applications of ET that are focused on the

ultrastructure of the intracellular membranes and provide a useful link to their function.

3.1.1. MITOCHONDRIA Prior to tomography, the ultrastructure of mitochondria was investigated essentially by two-dimensional EM of thin slices of conventionally prepared material. The consensus reached was the "baffle model," which describes the internal membrane of mitochondria as containing baffle-like involutions (cristae) with wide openings into the intermembrane compartment. It was essentially the ability of ET to produce three-dimensional representations that changed this view of the mitochondrial ultrastructure.

Because ET allowed the study of mitochondrial sections that were thick enough to contain a representative portion of the mitochondrial volume (0.2–1 μm), tomograms of conventionally prepared mitochondria showed that cristae have a pleomorphic structure, ranging from tubular to lamellar, and complicated topology. They are always connected to the periphery of the inner membrane via tubular connections (crista junctions). These findings marked the departure from the baffle model (83, 84). The new model of mitochondrial structure might lead to important conclusions about its function. It was proposed that the dynamic change of the shape of cristae might affect the concentration of cytochrome *c* and affect ATP production in vivo (84, 85).

Cryo-ET studies of mitochondria (85, 86) show smooth outer and inner membranes parallel to each other, as opposed to their rough appearance seen with the conventional and RF/FS methods (87). However, cryotomograms of isolated *Neurospora* mitochondria showed interconnected cristae and generally wider crista junctions (86), in contrast to the mitochondria in situ from the same organism (88). Although the differences might be artifacts of the conventional preparation, they could also be caused by the isolation procedure because mitochondria in the early stages of apoptosis are characterized by widening of cristae junctions and a lack of swelling (89). In principle, ET of mitochondrial cryo sections might provide the answer because it neither suffers from the artifacts of conventional preparation nor requires the isolation of mitochondria (129).

3.1.2. SECRETORY PATHWAY The study of the intricate membranous structure of secretory pathway elements, such as the Golgi complex, endosomes, and lysosomes, is another example of the capability of ET to provide us with data, which clearly outline a complex intracellular membrane structure. Membrane trafficking is a fast, dynamic process and suffers greatly from the slow rate of chemical fixation. The speed with which rapid freezing arrests the state of a Golgi complex in a cell and the ability of RF/FS to investigate sections of whole cells proved to be useful tools. Thus, RF/FS turned out to be the method of choice for investigation of the secretory pathway ultrastructure.

The Golgi complex consists of several flat membranous compartments (cisternae) organized in a stack with two distinct sides: the *cis* (usually oriented toward the nucleus) and the *trans* side. Newly synthesized proteins and lipids are

transported from the endoplasmic reticulum (ER) to the *cis* side of Golgi. They are covalently modified during their transport through the Golgi from *cis* toward *trans*, sorted, packed in transport vesicles, and released from the *trans* side to their destination.

Larger tomograms containing a complete Golgi stack, together with the neighboring ER and endosomal/lysosomal compartments, were obtained by combining either tomograms from neighboring sections or by individual projections from adjacent regions. Membranes of Golgi cisternae appear to be well preserved: They are smooth, straight, and parallel to each other. This allowed identification of all cisternae forming a Golgi complex (Figure 5), redefining what was known as the *trans* Golgi network, and provided the detailed characterization and interconnectivity of the tubules and budding processes emanating from them (90).

In mammalian Golgi, the combination of physiological manipulations and ET showed that the exit from Golgi occurs from three cisternae located on the *trans* side (91). Because of the exclusive presence of clathrin-coated buds on the *trans*-most cisterna and the nonclathrin-coated buds at the other two *trans*-cisternae (81), consistent with the results from budding yeast (92), it was predicted that the molecules targeted to different pathways leave from different cisternae (90). Under conditions that require large protein synthesis and secretion through Golgi, tubular connections between otherwise nonconnected cisternae at different levels were detected (93), pointing toward a dynamical regulation of the Golgi.

The appearance of similar structural features in ER-Golgi intermediate layer and in the *cis*-most Golgi cisterna, together with the observed fragmentation of the two most *trans*-cisternae, strengthened the hypothesis that the formation of new elements at the *cis* face of Golgi is coordinated with the consumption of *trans*-Golgi, commonly known as the cisternal progression/maturation model (94). Studies combining ET of RF/FS prepared cells with fluorescent microscopy and EM immunolabeling showed that transport from ER to Golgi occurs via the progressive extrusion of large ER domains (95), and that cargos of different sizes traverse the Golgi in a synchronous manner (96), which is consistent with the cisternal progression/maturation model.

Structural characterization of the tubular protrusions and internal structure of lysosomes and early and late endosomes showed that late endosomes contain isolated internal vesicles. A conclusion was made that the relocation of molecules from those vesicles to the cell surface includes a fusion between inner vesicles and the lysosomal outer membrane (67, 97).

3.2. Beyond Ultrastructure—From Organelles to Molecules

The structure of a molecular complex is closely related to its function. The applications of ET reviewed here go beyond the ultrastructure of internal membranes, toward structural investigations at the molecular level and their functional implications.

3.2.1. ORGANELLES INVOLVED IN CELL DIVISION AND MICROTUBULES ET of functional, isolated, conventionally prepared centrosomes showed many ring-shaped structures containing multiple copies of γ-tubulin, a key factor in microtubule nucleation (98). The main implication of these studies, that these γ-tubulin containing rings are the microtubule nucleation sites, were confirmed in (99). The structure of these rings directly supports the template model of microtubule nucleation, stating that the γ-tubulin ring provides a preformed start helix.

In an early example of cryo-ET, tomograms of the isolated core of a spindle pole body (SPB, a microtubule-organizing center in yeast, which is an equivalent of centrosome) were obtained (100). The structure of SPB was further investigated by RF/FS-prepared yeast cells (101). The microtubules of the mitotic spindle were tracked in various stages of spindle formation, but kinetochores, which were expected to be attached to the plus ends (ends opposite to SPB) of some of these microtubules, were not detected. New structures present in another type of a microtubule-organizing center (the basal body of alga *Chlamydomonas reinhardtii*) were found by combining ET with mutation studies (102).

Microtubules were successfully tracked from centrosomes to kinetochores in *Caenorhabditis elegans* embryo cells (103). Centrosome-associated microtubule ends were found in both capped and open states, the open-ended microtubules being preferentially associated with kinetochores. Presumably, the capped ends contain γ-tubulin and are stable, whereas the open ends reflect the dynamic state.

The ability of ET to investigate a cellular process whose manifestations occur simultaneously in a large area of a cell while retaining the resolution required to study organelles was shown in studies of cell wall formation in plants (104–106). A montage of neighboring projections allowed the reconstruction of tomograms representing large cellular volumes. These led to the discovery of new structural elements forming cell plates and more detailed three-dimensional structures of organelles involved in cell plate and cell wall assembly.

3.2.2. HIGHLY ORDERED STRUCTURES Averaging multiple copies of a structure of interest is one of the standard EM techniques used to reduce noise. Periodic structures such as many naturally occurring filaments are particularly suited for averaging because their periodicity provides a natural basis for averaging along the filament.

The periodicity of highly ordered arrays of actin and myosin fibers found by ET in insect flight muscle is a good example for the use of single-particle methods in ET as well as an example of the power of the structure-function approach. Tomograms of conventionally prepared insect flight muscle in rigor and nonrigor states show variable confirmations of actin-myosin cross bridges (107, 108). The three-dimensional information proved to be necessary for the precise localization of cross bridges. Of particular interest is the study using the RF/FS preparation (109). Rapid freezing of the contracting muscle preserved the wide variations of transient and variable cross-bridge conformations, as seen in the left panel of Figure 9. Individual filaments were averaged on the basis of their periodicity, and

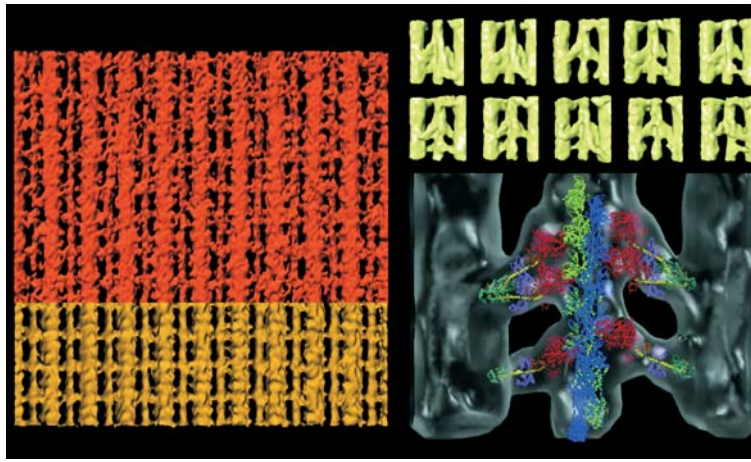

Figure 9 Insect flight muscle (from Reference 127, with permission, courtesy of Kenneth Taylor). (*left*) The upper (*copper-toned*) part shows an unaveraged tomogram, the lower (*gold*) part is the tomogram after column averaging. (*upper right*) Class averages display the variation found between individual actin-myosin cross bridges. (*lower right*) A pseudo-atomic model was obtained by docking atomic models into the class average motifs. The column repeat in the tomogram is 116 nm.

representative examples of these averages ("motifs") were found to represent the full range of cross-bridge arrangements (Figure 9, upper right). In addition, docking of the high-resolution structures of actin and myosin subfragment 1 into the motifs (Figure 9, lower right) led to the precise positioning of these structures and to a more precise description of the myosin power stroke. Improved methods for averaging and docking were developed, but they were used to analyze the tomograms obtained only from the conventionally prepared insect flight muscle. Instead of averaging single filaments, multivariate statistical analysis and self-organizing maps were used to classify different cross bridges, and the class averages were used as representative motifs (110–112). Refinement of the docking procedure by the introduction of hinge points in the myosin subfragment structure significantly reduced the number of residue clashes (111, 113). The docking procedure was hampered by the fact that high-resolution three-dimensional structures were fitted in the two-dimensional envelopes created by stain and by possible chemical fixation- and dehydration-induced conformation changes. However, reliable docking became possible with the use of averaging that decreases the noise and increases the resolution of envelopes used for docking.

Tomograms of negatively stained fibrillin-rich microfibrils, antibody mapping data, and measurements of mass distribution along fibrils under different states of tension were used, together with the fibrillin primary structure, to create a model of fibrillin alignment in microfibrils present in untensioned and stretched states (114).

3.2.3. NUCLEAR PORE COMPLEX—A CASE FOR AVERAGING The nuclear pore complex (NPC) is a large macromolecular complex of 125 MDa, with a diameter of 120 nm, embedded in the nuclear envelope. Because many NPCs can be present in a single tomogram, improved resolution of the NPC structure can be obtained by the averaging of properly aligned single NPCs

In two cryo-ET studies of NPC, three-dimensional representations of individual NPCs present in tomograms were averaged to reduce noise and to obtain an averaged structure. They both used native NPCs (obtained without detergents). In the first study, nuclei were opened manually, and the nuclear envelopes were spread (115). The structures of the pore itself and the nuclear plug/transporter were obtained. Because the nuclear envelopes were flattened, the main axis of all NPCs point in the same direction, perpendicular to the envelope. Consequently, the missing wedges of the individual NPC reconstructions upon averaging give rise to the missing cone and a lower resolution in the direction of the main axis. The second study (116) went a step further: Import competent NPCs were investigated directly on the intact nuclei, thus eliminating the opening of nuclei, which might cause disruption of NPCs. The NPCs were oriented in all directions, therefore the averaged structure does not suffer from the missing cone and is isotropic (Figure 10). Consequently, the averaged structure reached higher resolution and showed filaments that were not resolved in the earlier study. Furthermore, two

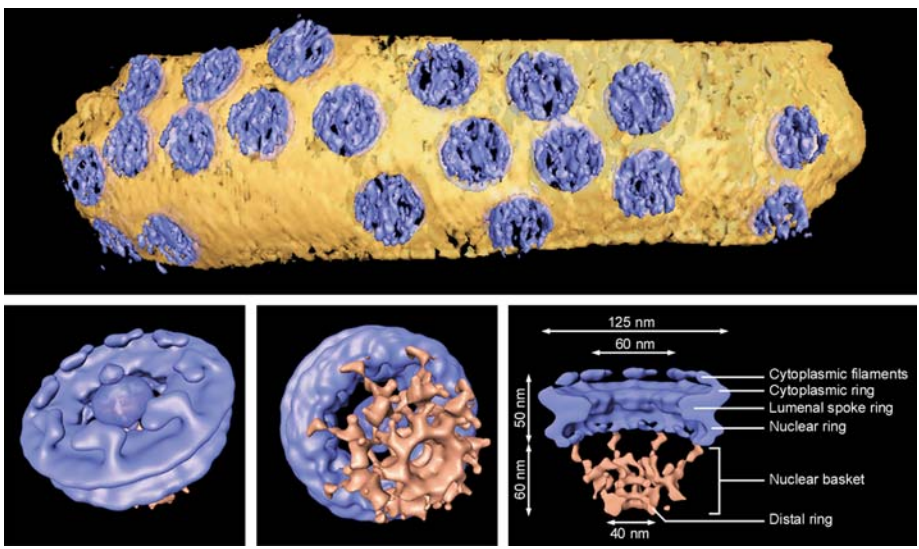

Figure 10 Nuclear pore complex (from Reference 116, with permission). (*top*) Isosurface representation of a tomogram showing the nuclear envelope. Individual NPCs (*purple*) and membrane (*yellow*) are segmented manually. (*bottom left and center*) Different views of averaged NPC structure. (*bottom right*) Overview of the structural elements of the NPC.

presumably functional states were detected, and the structures for each of them were obtained separately. This study is a significant achievement of cryo-ET, considering the sensitivity of cryo-ET on increased specimen thickness (the nuclei used here were 2 μm in diameter). Furthermore, the structures obtained form the platform for further studies of NPC in well-defined states, which are expected to result in three-dimensional snapshots of cargo in different stages of transit through the NPC.

3.2.4. VIRUSES—FROM SYMMETRICAL TO PLEOMORPHIC STRUCTURES The highly symmetrical three-dimensional structure of many viruses makes them suitable for EM investigations using single-particle methodology. However, many viruses, such as human immunodeficiency virus (HIV), are entirely pleomorphic. ET is a suitable technique for three-dimensional imaging of both classes at high resolution in toto.

Recently, ET has been used to study HIV and simian immunodeficiency virus (SIV) (117). Although the flattening of the viruses, resulting from the staining procedure followed by air drying, limited the structural insights obtained, this study provided novel information. The number and the distribution of envelope protein complexes (Env), which mediate the fusion between virus and host cell, were determined, and their structural surfaces were characterized.

The structural interpretation of cryo-prepared viruses is not limited to particular aspects such as the envelope proteins. Studies on phages showed that structural features up to 3 nm are contained in cryotomograms of viruses (118). Cryo-ET of intact virions of Herpes simplex virus nicely illustrates the power of cryo-ET at the molecular level (119). It provided novel information about the pleomorphic structures that are crucial for infection of host cells: tegument and embedded glycoproteins of the envelope (Figure 11). It also showed that the highly symmetrical nucleocapsid adopts an eccentric position within the approximately spherical virus. Furthermore, the nucleocapsids were extracted from tomograms, averaged, and compared to the nontegumented capsid, revealing nucleocapsid-tegument contacts.

A study of an entirely nonsymmetrical vaccinia virus revealed a complex shell consisting of different layers, in which the inner core membrane incorporates pore-like formations (120). The structure of membrane-bound Env complexes from Moloney murine leukemia virus was obtained from tomograms of entire virions by averaging. The resolution (below 3 nm) is on the verge of allowing to fit an X-ray structure unambiguously into the Env complex structure (65).

3.2.5. IDENTIFICATION OF MEMBRANE-BOUND MOLECULES The known cellular localization of many molecules and complexes can be an important factor in their identification in tomograms. The location of transmembrane- and membrane-associated proteins is particularly useful in this respect because membranes are usually easily identifiable and the space surrounding membranes is small in respect to the whole tomogram, thus reducing the volume to be searched.

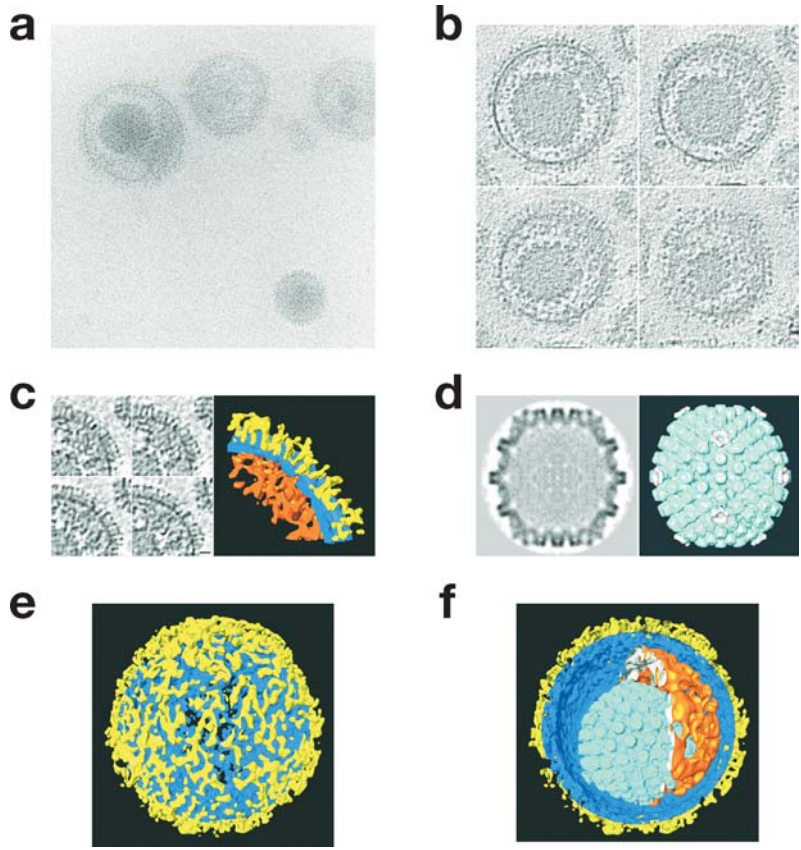

Figure 11 Cryo-ET of the pleomorphic herpes simplex virus 1 (HSV-1) virions (from Reference 119, with permission). (*a*) Projection showing the icosahedral capsid harboring the dsDNA (*lower right*), the membrane-bound and capsid-containing infectious particle, the virion (*upper left*), and the membrane-bound "light" particles lacking a capsid, the "L-particles" (*upper right*). (*b*) Denoised tomographic slices (20-nm spacing). (*c*) Denoised and volume-rendered representation of a segment of the envelope and tegument. (*d*) Averaged and symmetrized structure of the icosahedral (T6) nucleocapsid. (*e*, *f*) The refined capsid structure was docked into the denoised overall tomogram of the virion, generating a synthetic tomogram.

Tomograms of the presynaptic side of a RF/FS-prepared frog neuromuscular junction show membrane-attached densities close to presynaptic vesicles docked to the membrane (122). On the basis of their localization, these densities were tentatively identified as voltage-gated Ca^{2+} channels. The small size of protein constituents of the presynaptic exocytotic machinery and the limitations of the RF/FS preparation do not allow accurate molecular identification. Cryotomograms

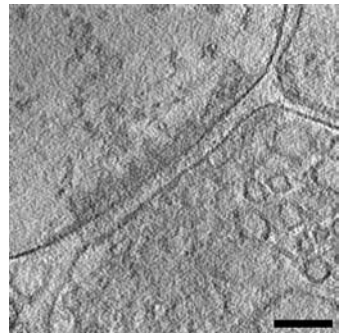

Figure 12 Cryo-ET of an excitatory synapse from a synaptosomal cellular fraction denoised with the bilateral filter. (*upper left*) Postsynaptic terminal with postsynaptic density. (*lower right*) Presynaptic terminal. Scale bar 100 nm.

of synapses from the central nervous system obtained from the synaptosomal cellular fraction show a plethora of structurally different transmembrane proteins and might provide us with more information about the organization of synaptic complexes (130) (Figure 12).

Identification of molecules, using their structural signature, in tomograms holds a great promise for the future. The first steps in combining this approach with membrane localization properties have already been taken. Cryotomograms of inside-out vesicles, formed by resealing of the inner membrane of disrupted mitochondria, contain a clearly visible array of particles sticking out of the membrane. Considering the overall shape of these particles and their location, they are probably ATP synthases (86). In another example, cryotomograms of triad junctions from the microsomal cellular fraction showed structures protruding from the membranes of the sarcoplasmic reticulum. Their location was consistent with ryanodine receptors, large Ca^{2+} permeable channels of 2.3 MDa (123) (Figure 13). This identification was confirmed by the use of software for molecular identification (124).

3.2.6. CRYO-ET OF WHOLE CELLS Whole-cell imaging by cryo-ET combines the best structural preservation with the ability to observe intact molecular complexes in their unperturbed native environment. A lot of fundamental biological questions can be answered by investigating whole bacteria, and many eukaryotic cells are amenable to cryo-ET.

Tomograms of bacterium *Spiroplasma melliferum* at 4 nm resolution allowed the detection of its cytoskeleton and its components (Figure 14) (125). The cytoskeleton was found to consist of three parallel ribbons running through the whole cell, each ribbon containing either thin (4 nm) or thick (9 nm) filaments, raising new questions about the molecular composition of the filaments and the mechanistic basis of motility.

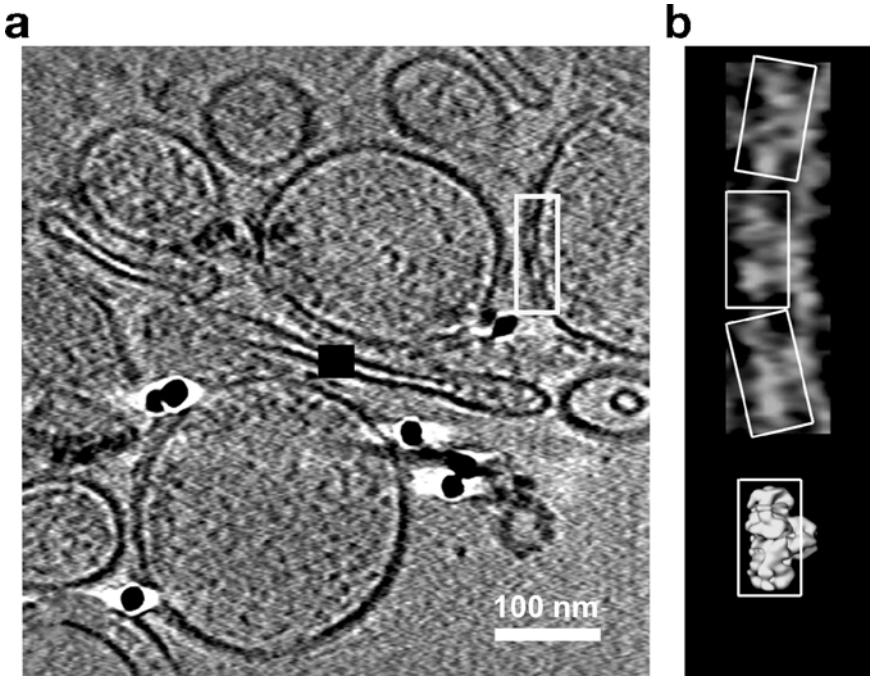

Figure 13 Identification of ryanodine receptors based on their known membrane localization and large size (2.3 MDa) (from Reference 123, with permission). (*A*) Tomographic slice of cryoprepared isolated triad junction. The boxed area containing ryanodine receptors is shown in (*B*) (in inverse contrast), together with the structure of the isolated receptor.

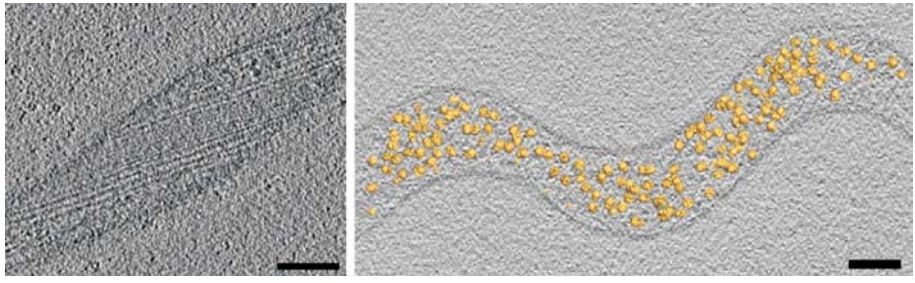

Figure 14 Cryo-ET of *Spiroplasma melliferum*. (*left*) Tomographic slice with clearly identifiable cytoskeleton (from Reference 125, with permission). (*right*) Ribosomes were identified using molecular identification software (J. Ortiz & W. Baumeister, unpublished results). Scale bars 100 nm.

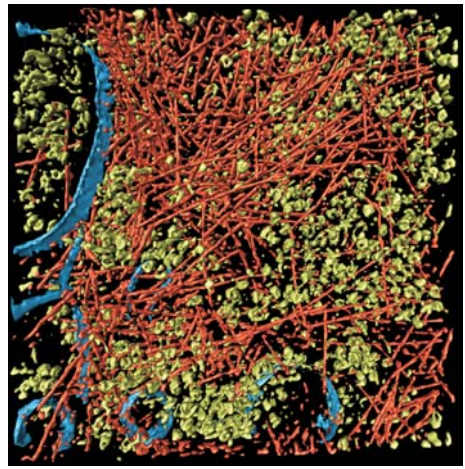

Figure 15 Visualization of the actin network (*red*) and cytoplasmic complexes (*green*) from a cryo-ET of *Dicyostelium* (from Reference 56, with permission).

The generally larger size of eukaryotic cells restricts the application of cryo-ET to their flat parts. This possibility was explored in tomograms of peripheral regions of *Dictyostelium* cells (56). The highly dynamic actin network of these cells was arrested within milliseconds by rapid freezing, making the tomograms faithful snapshots of the actin state, and allowing the detailed investigation of the arrangement and branching of actin filaments, their interaction with the cell membrane, as well as the structure of the membrane attachment sites (Figure 15).

The relatively noncrowded nature of *Dictyostelium* cytoplasm allowed the identification of the 26S proteasome complexes on the basis of their structural signature in this study. Also, ribosomes were mapped in the tomograms of *S. melliferum* by the molecular identification software based on pattern matching (Figure 14) (J. Ortiz, W. Baumeister, unpublished results). The fact that a cytoplasmic molecular complex can be unambiguously identified in its natural environment with purely structural information clearly shows the tremendous potential of cryo-ET of whole eukaryotic cells for the investigation of cellular processes at the molecular level. It also confirms that an imposing amount of data is present in the cryotomograms and provides an incentive for further cryo-ET studies of whole cells, as well as for the development of software tools that allow comprehensive and objective analysis of that data.

4. CONCLUSION

Following slow initial development over several decades, ET has gathered momentum in the recent years. Studies of cells that provided complex membrane structures of organelles and made important structural and functional advances,

benefited greatly from the recent improvements in specimen preparation. The RF/FS preparation provides good contrast and is a significant improvement over the conventional method, and very importantly, it is applicable to whole cells and tissues. The resolution obtained in the tomograms is mainly limited by the inaccuracy of the representation of the biological material. Therefore, although RF/FS is not adequate for molecular investigation, it is currently the method of choice for ET investigations of ultrastructure and large supramolecular assemblies within whole cells and tissues.

Cryo-ET provides reliable structural information of cells at the molecular level. Molecules, complexes, and supramolecular assemblies can be imaged using cryo-ET in their native state and their natural environment; the structure of cryo-prepared material is perfectly preserved. Furthermore, a molecule is represented by a three-dimensional map that faithfully represents both its surface and internal structure. Cryo-ET is suitable for thin specimens, such as isolated complexes, small cells, and thin regions of larger cells, including many eukaryotic cells. New strategies for protein purification, especially strategies more concerned with the preservation of weakly bound and transient complexes than with purification, are needed to extend the cryo-ET range of applications.

Cryosectioning holds the promise to combine the best of two worlds, allowing the investigation of whole cells preserved in a close to physiological state. Despite the significant progress made in cryosectioning, it currently is by no means a routine preparation, and it is yet to reach its full potential.

The interplay of the electron dose and noise sets the fundamental limitation of cryo-ET. Because radiation damage limits the electron dose, noise is necessarily present in the tomograms, and it effectively limits the usable resolution. Cryotomograms contain information up to the resolution limits set by the instrumentation and reconstruction procedure, albeit obscured by noise. Because the biological structures are faithfully represented, an enormous amount of information is provided, and extracting this information becomes crucial.

Clearly, quantitative computational methods are needed. Sophisticated denoising algorithms are designed to reduce noise and increase the usable resolution. Automatic segmentation algorithms could be used to extract membranes, uncover filamental structures, and discern their organization. Some of the problems in the interpretation of tomograms will disappear once a resolution of 2 to 3 nm is obtained. At this resolution, reliable docking of high-resolution structures yielding pseudo-atomic maps of molecular complexes will become straightforward. In addition, these computational methods might be complemented by information provided by other approaches and information, such as localization, labeling studies, and the binding properties of molecules.

Cryo-ET of whole cells allows us to investigate the structure-function relationship of molecular complexes and supramolecular assemblies in their native environment. It thus makes a fundamental change in the way we approach biochemical processes that underlie and orchestrate higher cellular functions. In the past, molecular interactions were studied mostly in a collective manner, whereas

now we have the tools to visualize the interactions between individual molecules in their unperturbed functional environments. Although they share common underlying principles, no two cells or organelles are identical, owing to the inherent stochasticity of biochemical processes in cells as well as their functional diversity. Therefore, it will be a major challenge to extract generic features from the maps, such as the modes of interaction between molecular species. The ultimate goal, the discovery of general rules that underlie cellular processes, has to go beyond observing qualitative features and has to be based on stringent analytical criteria.

ACKNOWLEDGMENT

We thank Gabriela J. Greif and Andrew Leis for critical reading of the manuscript.

The *Annual Review of Biochemistry* is online at http://biochem.annualreviews.org

LITERATURE CITED

1. Radon J. 1917. *Ber. Sächs. Akad. Wiss. Leipzig, Math.-Phys. Kl.* 69:262–77
2. DeRosier DJ, Klug A. 1968. *Nature* 217:130–34
3. Hart RG. 1968. *Science* 159(822):1464–67
4. Baumeister W, Grimm R, Walz J. 1999. *Trends Cell Biol.* 9(2):81–85
5. Matricardi VR, Moretz RC, Parsons DF. 1972. *Science* 177(45):268–70
6. Fernandez-Moran H. 1960. *Ann. NY Acad. Sci.* 85:689–713
7. Taylor KA, Glaeser RM. 1974. *Science* 186(4168):1036–37
8. Dubochet J, Adrian M, Chang JJ, Homo JC, Lepault J, et al. 1988. *Q. Rev. Biophys.* 21(2):129–228
9. Typke D, Dierksen K, Baumeister W. 1991. Automatic electron tomography. *Proc. 49th Annu. Meet., EMSA*, pp. 544–45. San Francisco, CA: San Francisco Press
10. Dierksen K, Typke D, Hegerl R, Koster A, Baumeister W. 1992. *Ultramicroscopy* 40:71–87
11. Koster AJ, Chen H, Sedat JW, Agard DA. 1992. *Ultramicroscopy* 46(1–4):207–27
12. Misell D, Burdett I. 1977. *J. Microsc.* 109:171–82
13. Hawkes P. 1992. See Ref. 128, pp. 17–38
14. Toyoshima C, Unwin N. 1988. *Ultramicroscopy* 25:279–92
15. Grimm R, Koster AJ, Ziese U, Typke D, Baumeister W. 1996. *J. Microsc.* 183:60–68
16. Grimm R, Bärmann M, Häckl W, Typke D, Sackmann E, Baumeister W. 1997. *Biophys. J.* 72:482–89
17. Grimm R, Singh H, Rachel R, Typke D, Zillig W, Baumeister W. 1998. *Biophys. J.* 74(2 Part 1):1031–42
18. Fan GY, Ellisman MH. 2000. *J. Microsc.* 200(Part 1):1–13
19. Fan GY, Ellisman MH. 1993. *Ultramicroscopy* 52(1):21–29
20. Fan GY, Datte P, Beuville E, Beche JF, Millaud J, et al. 1998. *Ultramicroscopy* 70(3):107–13
21. Dierksen K, Typke D, Hegerl R, Baumeister W. 1993. *Ultramicroscopy* 49:109–20
22. Dierksen K, Typke D, Hegerl R, Walz J, Sackmann E, Baumeister W. 1995. *Biophys. J.* 68(4):1416–22
23. Koster AJ, de Ruijter WJ, van den Bos A, van der Mast KD. 1989. *Ultramicroscopy* 27:251–72
24. Ziese U, Geerts WJ, Van der Krift TP,

Verkleij AJ, Koster AJ. 2003. *J. Microsc.* 211(Part 2):179–85
25. Ziese U, Janssen AH, Murk JL, Geerts WJ, Van der Krift T, et al. 2002. *J. Microsc.* 205(Part 2):187–200
26. Zheng QS, Braunfeld MB, Sedat JW, Agard DA. 2004. *J. Struct. Biol.* 147(2): 91–101
27. Guckenberger R. 1982. *Ultramicroscopy* 9:167–74
28. Liu Y, Penczek P, McEwen B, Frank J. 1995. *Ultramicroscopy* 58:393–402
29. Taylor KA, Tang J, Cheng Y, Winkler H. 1997. *J. Struct. Biol.* 120(3):372–86
30. Lawrence M. 1992. See Ref. 128, pp. 197–204
31. Hoppe W, Hegerl R. 1980. In *Computer Processing of Electron Microscope Images*, ed. PW Hawkes, pp. 127–85. Berlin/Heidelberg/New York:Springer-Verlag
32. Radermacher M. 1992. See Ref. 128, pp. 91–115
33. Harauz G, van Heel M. 1986. *Optik* 73:146–56
34. Gordon R, Bender R, Herman GT. 1970. *J. Theor. Biol.* 29(3):471–81
35. Crowther RA, Klug A. 1971. *J. Theor. Biol.* 32(1):199–203
36. Carazo J. 1992. See Ref. 128, pp. 117–66
37. Penczek P, Radermacher M, Frank J. 1992. *Ultramicroscopy* 40:33–53
38. Marabini R, Rietzel E, Schroeder R, Herman G, Carazo J. 1997. *J. Struct. Biol.* 120:363–71
39. Skoglund U, Ofverstedt LG, Burnett RM, Bricogne G. 1996. *J. Struct. Biol.* 117(3):173–88
40. Fernandez JJ, Lawrence AF, Roca J, Garcia I, Ellisman MH, Carazo JM. 2002. *J. Struct. Biol.* 138(1–2):6–20
41. Hegerl R, Hoppe W. 1976. *Z. Naturforsch. Teil A* 31a:1717–21
42. McEwen B, Downing K, Glaeser R. 1995. *Ultramicroscopy* 60:357–73
43. Saxberg B, Saxton W. 1981. *Ultramicroscopy* 6:85–90
44. Crowther R, DeRosier D, Klug A. 1970. *Proc. R. Soc. London Ser. A* 317:319–40
45. Saxton W, Baumeister W, Hahn M. 1984. *Ultramicroscopy* 13:57–70
46. Mastronarde DN. 1997. *J. Struct. Biol.* 120(3):343–52
47. Nickell S, Hegerl R, Baumeister W, Rachel R. 2003. *J. Struct. Biol.* 141(1):34–42
48. Penczek P, Marko M, Buttle K, Frank J. 1995. *Ultramicroscopy* 60:393–410
49. Frangakis A, Hegerl R. 2002. *J. Struct. Biol.* 138:105–13
50. Volkmann N. 2002. *J. Struct. Biol.* 138(1–2):123–29
51. Frangakis AS, Forster F. 2004. *Curr. Opin. Struct. Biol.* 14(3):325–31
52. Frangakis A, Hegerl R. 2001. *J. Struct. Biol.* 135(3):239–50
53. Fernandez JJ, Li S. 2003. *J. Struct. Biol.* 144(1–2):152–61
54. Jiang W, Baker ML, Wu Q, Bajaj C, Chiu W. 2003. *J. Struct. Biol.* 144(1–2):114–22
55. Stoschek A, Hegerl R. 1997. *J. Struct. Biol.* 120:257–65
56. Medalia O, Weber I, Frangakis AS, Nicastro D, Gerisch G, Baumeister W. 2002. *Science* 298(5596):1209–13
57. Böhm J, Frangakis AS, Hegerl R, Nickell S, Typke D, Baumeister W. 2000. *Proc. Natl. Acad. Sci. USA* 97(26):14245–50
58. Frangakis AS, Bohm J, Forster F, Nickell S, Nicastro D, et al. 2002. *Proc. Natl. Acad. Sci. USA* 99(22):14153–58
59. Sali A, Glaeser R, Earnest T, Baumeister W. 2003. *Nature* 422(6928):216–25
60. Roseman AM. 2000. *Acta Crystallogr. D* 56:1332–40
61. Roseman AM. 2003. *Ultramicroscopy* 94(3–4):225–36
62. Rath BK, Hegerl R, Leith A, Shaikh TR, Wagenknecht T, Frank J. 2003. *J. Struct. Biol.* 144(1–2):95–103
63. Walz J, Tamura T, Tamura N, Baumeister W, Grimm R, Koster A. 1997. *Mol. Cell* 1(1):59–65
64. Nitsch M, Walz J, Typke D, Klumpp M, Essen LO, Baumeister W. 1998. *Nat. Struct. Biol.* 5(10):855–57
65. Förster F, Medalia O, Zauberman N,

Baumeister W, Fass D. 2005. *Proc. Natl. Acad. Sci. USA* 102:4729–34
66. Moor H. 1987. In *Cryotechniques in Biological Electron Microscopy*, ed. RA Steinbrecht, K Zierold, pp. 175–91. Berlin: Springer-Verlag
67. Murk JL, Posthuma G, Koster AJ, Geuze HJ, Verkleij AJ, et al. 2003. *J. Microsc.* 212(Part 1):81–90
68. Dubochet J, Blanc NS. 2001. *Micron* 32:91–99
69. McIntosh JR. 2001. *J. Cell Biol.* 153(6): F25–32
70. Al-Amoudi A, Dubochet J, Gnaegi H, Luthi W, Studer D. 2003. *J. Microsc.* 212(Part 1):26–33
71. Al-Amoudi A, Norlen LP, Dubochet J. 2004. *J. Struct. Biol.* 148(1):131–35
72. He W, Cowin P, Stokes DL. 2003. *Science* 302(5642):109–13
73. Tokuyasu KT. 1973. *J. Cell Biol.* 57(2): 551–65
74. Monaghan P, Perushinghe N, Müller M. 1998. *J. Microsc.* 192(3):248–58
75. Koster AJ, Klumperman J. 2003. *Nat. Rev. Mol. Cell Biol.* 4(Suppl.):S6–10
76. Gaietta G, Deerinck TJ, Adams SR, Bouwer J, Tour O, et al. 2002. *Science* 296(5567):503–7
77. Talmon Y. 1987. In *Electron Beam Radiation Damage to Organic and Biological Cryospecimens*, ed. RA Steinbrecht, K Zierold, pp. 64–86. Berlin: Springer-Verlag
78. McEwen BF, Marko M, Hsieh CE, Mannella C. 2002. *J. Struct. Biol.* 138(1–2): 47–57
79. Winkler H, Taylor KA. 2003. *J. Struct. Biol.* 143(1):24–32
80. Luther PK. 1992. See Ref. 128, pp. 39–62
81. Ladinsky MS, Mastronarde DN, McIntosh JR, Howell KE, Staehelin LA. 1999. *J. Cell Biol.* 144(6):1135–49
82. McEwen BF, Marko M. 2001. *J. Histochem. Cytochem.* 49(5):553–64
83. Perkins GA, Frey TG. 2000. *Micron* 31(1):97–111
84. Frey TG, Mannella CA. 2000. *Trends Biochem. Sci.* 25(7):319–24
85. Mannella CA, Pfeiffer DR, Bradshaw PC, Moraru II, Slepchenko B, et al. 2001. *IUBMB Life* 52(3–5):93–100
86. Nicastro D, Frangakis AS, Typke D, Baumeister W. 2000. *J. Struct. Biol.* 129(1):48–56
87. Perkins GA, Song JY, Tarsa L, Deerinck TJ, Ellisman MH, Frey TG. 1998. *J. Bioenerg. Biomembr.* 30(5):431–42
88. Perkins GA, Renken CW, van der Klei IJ, Ellisman MH, Neupert W, Frey TG. 2001. *Eur. J. Cell Biol.* 80(2):139–50
89. Scorrano L, Ashiya M, Buttle K, Weiler S, Oakes SA, et al. 2002. *Dev. Cell* 2(1):55–67
90. Mogelsvang S, Marsh BJ, Ladinsky MS, Howell KE. 2004. *Traffic* 5(5):338–45
91. Ladinsky MS, Wu CC, McIntosh S, McIntosh JR, Howell KE. 2002. *Mol. Biol. Cell* 13(8):2810–25
92. Mogelsvang S, Gomez-Ospina N, Soderholm J, Glick BS, Staehelin LA. 2003. *Mol. Biol. Cell* 14(6):2277–91
93. Marsh BJ, Volkmann N, McIntosh JR, Howell KE. 2004. *Proc. Natl. Acad. Sci. USA* 101(15):5565–70
94. Marsh BJ, Mastronarde DN, McIntosh JR, Howell KE. 2001. *Biochem. Soc. Trans.* 29(Part 4):461–67
95. Mironov AA, MironovAA Jr, Beznoussenko GV, Trucco A, Lupetti P, et al. 2003. *Dev. Cell* 5(4):583–94
96. Mironov AA, Beznoussenko GV, Nicoziani P, Martella O, Trucco A, et al. 2001. *J. Cell Biol.* 155(7):1225–38
97. Murk JL, Humbel BM, Ziese U, Griffith JM, Posthuma G, et al. 2003. *Proc. Natl. Acad. Sci. USA* 100(23):13332–37
98. Moritz M, Braunfeld MB, Sedat JW, Alberts B, Agard DA. 1995. *Nature* 378(6557):638–40
99. Moritz M, Braunfeld MB, Guenebaut V, Heuser J, Agard DA. 2000. *Nat. Cell Biol.* 2(6):365–70
100. Bullitt E, Rout MP, Kilmartin JV, Akey CW. 1997. *Cell* 89(7):1077–86

101. O'Toole ET, Winey M, McIntosh JR. 1999. *Mol. Biol. Cell* 10(6):2017–31
102. O'Toole ET, Giddings TH, McIntosh JR, Dutcher SK. 2003. *Mol. Biol. Cell* 14(7):2999–3012
103. O'Toole ET, McDonald KL, Mantler J, McIntosh JR, Hyman AA, Muller-Reichert T. 2003. *J. Cell Biol.* 163(3): 451–56
104. Otegui MS, Mastronarde DN, Kang BH, Bednarek SY, Staehelin LA. 2001. *Plant Cell* 13(9):2033–51
105. Otegui MS, Staehelin LA. 2004. *Planta* 218(4):501–15
106. Segui-Simarro JM, White EA, Staehelin LA. 2004. *Plant Cell* 16(4):836–56
107. Schmitz H, Reedy MC, Reedy MK, Tregear RT, Winkler H, Taylor KA. 1996. *J. Mol. Biol.* 264(2):279–301
108. Schmitz H, Reedy MC, Reedy MK, Tregear RT, Taylor KA. 1997. *J. Cell Biol.* 139(3):695–707
109. Taylor KA, Schmitz H, Reedy MC, Goldman YE, Franzini-Armstrong C, et al. 1999. *Cell* 99(4):421–31
110. Winkler H, Taylor KA. 1999. *Ultramicroscopy* 77(3–4):141–52
111. Chen LF, Winkler H, Reedy MK, Reedy MC, Taylor KA. 2002. *J. Struct. Biol.* 138(1–2):92–104
112. Pascual-Montano A, Taylor KA, Winkler H, Pascual-Marqui RD, Carazo JM. 2002. *J. Struct. Biol.* 138(1–2):114–22
113. Chen LF, Blanc E, Chapman MS, Taylor KA. 2001. *J. Struct. Biol.* 133(2–3):221–32
114. Baldock C, Koster AJ, Ziese U, Rock MJ, Sherratt MJ, et al. 2001. *J. Cell Biol.* 152(5):1045–56
115. Stoffler D, Feja B, Fahrenkrog B, Walz J, Typke D, Aebi U. 2003. *J. Mol. Biol.* 328(1):119–30
116. Beck M, Förster F, Ecke M, Plizko J, Melhior F, et al. 2004. *Science* 306(5700):1387–90
117. Zhu P, Chertova E, Bess JJ, Lifson JD, Arthur LO, et al. 2003. *Proc. Natl. Acad. Sci. USA* 100(26):15812–17
118. Bohm J, Lambert O, Frangakis AS, Letellier L, Baumeister W, Rigaud JL. 2001. *Curr. Biol.* 11(15):1168–75
119. Grunewald K, Desai P, Winkler DC, Heymann JB, Belnap DM, et al. 2003. *Science* 302(5649):1396–98
120. Cyrklaff M, Risco C, Fernández JJ, Jiménez MV, Estéban M, et al. 2005. *Proc. Natl. Acad. Sci. USA* 102:2772–77
121. Förster F, Baumeister W. 2004. Deleted in proof
122. Harlow ML, Ress D, Stoschek A, Marshall RM, McMahan UJ. 2001. *Nature* 409(6819):479–84
123. Wagenknecht T, Hsieh CE, Rath BK, Fleischer S, Marko M. 2002. *Biophys. J.* 83(5):2491–501
124. Rath BK, Hegerl R, Leith A, Shaikh TR, Wagenknecht T, Frank J. 2003. *J. Struct. Biol.* 144(1–2):95–103
125. Kürner J, Frangakis AS, Baumeister W. 2005. *Science* 307(5708):436–38
126. Deleted in proof
127. Baumeister W. 2002. *Curr. Opin. Struct. Biol.* 12(5):679–84
128. Frank J, ed. 1992. *Electron Tomography*. New York: Plenum
129. Hsieh C-E, Marko M, Frank J, Mannella CA. 2002. *J. Struct. Biol.* 138:63–73
130. Lučić V, Yang T, Schweikert G, Förster F, Baumeister W. 2005. *Structure* 13:423–34

Annual Review of Biochemistry
Volume 74, 2005

CONTENTS